Title

Neuron-Targeted Caveolin-1 Promotes Ultrastructural and Functional Hippocampal Synaptic Plasticity

Journal

Cerebral Cortex, 28(9)

ISSN

1047-3211

Authors

Egawa, Junji

Zemljic-Harpf, Alice

Mandyam, Chitra D

et al.

Publication Date

2018-09-01

DOI

10.1093/cercor/bhx196

Peer reviewed

Cerebral Cortex, September 2018;28: 3255–3266

doi: 10.1093/cercor/bhx196
Advance Access Publication Date: 31 July 2017
Original Article

ORIGINAL ARTICLE

Neuron-Targeted Caveolin-1 Promotes Ultrastructural and Functional Hippocampal Synaptic Plasticity

Junji Egawa[1,2], Alice Zemljic-Harpf[1,2], Chitra D. Mandyam[1,2], Ingrid R. Niesman[4], Larisa V. Lysenko[3], Alexander M. Kleschevnikov[3], David M. Roth[1,2], Hemal H. Patel[1,2], Piyush M. Patel[1,2] and Brian P. Head[1,2]

[1]Veterans Affairs San Diego Healthcare System, San Diego, CA 92161, USA, [2]Department of Anesthesiology, School of Medicine, University of California, San Diego, La Jolla, CA 92093, USA, [3]Department of Neurosciences, University of California, San Diego, La Jolla, CA 92093, USA and [4]Sanford-Burnham Medical Research Institute, La Jolla, CA 92037, USA

Address correspondence to Brian P. Head, Department of Anesthesiology, University of California, San Diego, VASDHS (9125), 3350 La Jolla Village Dr., San Diego, CA 92161, USA. Email: bhead@ucsd.edu

Abstract

A delicate interneuronal communication between pre- and postsynaptic membranes is critical for synaptic plasticity and the formation of memory. Evidence shows that membrane/lipid rafts (MLRs), plasma membrane microdomains enriched in cholesterol and sphingolipids, organize presynaptic proteins and postsynaptic receptors necessary for synaptic formation and signaling. MLRs establish a cell polarity that facilitates transduction of extracellular cues to the intracellular environment. Here we show that neuron-targeted overexpression of an MLR protein, caveolin-1 (*SynCav1*), in the adult mouse hippocampus increased the number of presynaptic vesicles per bouton, total excitatory type I glutamatergic synapses, number of same-dendrite multiple-synapse boutons, increased myelination, increased long-term potentiation, and increased MLR-localized *N*-methyl-D-aspartate receptor subunits (GluN1, GluN2A, and GluN2B). Immunogold electron microscopy revealed that Cav-1 localizes to both the pre- and postsynaptic membrane regions as well as in the synaptic cleft. These findings, which are consistent with a significant increase in ultrastructural and functional synaptic plasticity, provide a fundamental framework that underlies previously demonstrated improvements in learning and memory in adult and aged mice by *SynCav1*. Such observations suggest that Cav-1 and MLRs alter basic aspects of synapse biology that could serve as potential therapeutic targets to promote neuroplasticity and combat neurodegeneration in a number of neurological disorders.

Key words: electron microscopy, long-term potentiation, myelination, ultrastructure, NMDAR

Introduction

The term “synaptic plasticity” was first described by the Polish psychologist Jerzy Konorski in the 1940s as persistent, activity driven alterations in synaptic efficacy to be the foundation of information storage in the brain (Konorski 1948). Decades later in the 1960s Terje Lomo and Tim Bliss, working for Per Anderson’s laboratory at the University of Oslo made a major advancement on this concept by demonstrating that successive tetanic stimuli of increasing frequency resulted in a potentiated response, a term known as long-lasting potentiation (later changed to long-term potentiation or LTP by Graham Goddard) (Andersen 1960; Bliss and Lomo 1973; Douglas and Goddard 1975). The most studied classical aspect of LTP is the Hebbian form of synaptic plasticity, which involves the perforant path

originating from the entorhinal cortex innervating dentate gyrus (DG) granule cells, and the cornu ammonis (CA)3 Schaffer collateral axons which terminate on CA1 pyramidal cell dendrites. Stimuli of either pathway induce persistent and long-lasting increases in synaptic responses (hours to days) (Abraham 2003) and are heavily dependent upon neurotransmitter release from the presynaptic (PS) cleft and activation of ligand and voltage-dependent *N*-methyl-D-aspartate receptors (NMDARs) on the postsynaptic membrane (Andersen et al. 2007). Events that lead to synaptic plasticity (e.g., LTP, environment enrichment, formation of new memories) are indicated morphologically by ultrastructural changes including growth of new spines, changes in the structure of existing spines (Bourne and Harris 2011), increases in the proportion of single axonal boutons synapsing onto multiple dendritic spines from the same dendrite (same-dendrite multiple-synapse boutons [dsMSBs] (Fiala et al. 2002)), and the presence of smooth endoplasmic reticulum associated with electron-dense polyribosomes (Geinisman 1993; Spacek and Harris 1997; Cooney et al. 2002; Ostroff et al. 2002; Bourne and Harris 2011). Although decades of research have yielded a better understanding of the molecular and subcellular events leading to synaptic plasticity, how these events are initiated or regulated is not completely known. Therefore, understanding the molecular components that (1) regulate vesicular trafficking of presynaptic vesicles (PSVs) to the target PS membrane and (2) modulate postsynaptic membrane localization of key receptors and their associated signaling complement may identify molecular targets for restoring or even enhancing functional synaptic plasticity and improve cognitive function in animal models of neurodegenerative diseases.

Evidence shows that proteins involved in neurotransmission and synaptic plasticity localize to membrane/lipid rafts (MLRs) (Head et al. 2014; Liu et al. 2013; Egawa et al. 2016; Madwar et al. 2016). MLRs are plasmalemmal microdomains enriched in cholesterol, sphingolipids, and scaffolding proteins such as caveolins (Cavs) (Head et al. 2014). Together, Cav-1 and MLR organize a multitude of synaptic receptors (Delint-Ramirez et al. 2008; Head et al. 2008, 2011, 2014), small GTPases that modulate cytoskeletal-membrane tethering and dynamics (Head et al. 2006; Del Pozo and Schwartz 2007; Grande-Garcia and del Pozo 2008; de Kreuk et al. 2011), and PS proteins necessary for exocytosis and neurotransmitter release (Gil et al. 2005; Garcia-Martinez et al. 2015). Moreover, MLR have been shown to be critical for neuritogenesis, axonal guidance (Denny 2006; Guirland and Zheng 2007), and synapse formation/stabilization (Da Silva et al. 2005; Kamiguchi 2006; Willmann et al. 2006; Liu et al. 2013; Madwar et al. 2016). Loss or disruption of MLR from the leading edge results in growth cone collapse and inhibition of neuritogenesis (Nakai and Kamiguchi 2002; Niethammer et al. 2002). We have previously shown that neuron-targeted overexpression of Cav-1 using a synapsin promoter (termed *SynCav1*) enhanced MLR formation, increased pro-growth signaling (Trk signaling, receptor-mediated cAMP formation), increased molecular markers of synaptic plasticity (PSD95, synaptobrevin, syntaxin, synaptophysin [SYNPHYS]), and promoted dendritic growth and arborization in primary rodent neurons and in human neurons derived from induced pluripotent stem cells (iPSCs) in vitro (Head et al. 2011; Kassan et al. 2017). The significance of these findings was further substantiated when delivery of *SynCav1* to the hippocampus augmented structural plasticity and improved learning and memory dependent on the hippocampus in both adult and aged mice (Mandyam et al. 2017). Moreover, our neuron-targeted Cav-1 transgenic mouse (SynCav1 Tg) exhibited preserved hippocampal-dependent learning and memory and improved motor function recovery months after brain trauma (Egawa et al. 2017).

The present findings demonstrate that *SynCav1* delivery to the hippocampus in vivo augments synaptic plasticity as indicated by increases in total synapses, number of PSVs per bouton, total splitting synapse boutons, and increases myelination, all of which are gross anatomical and microscopic indicators of structural neuroplasticity. These neuroplastic alterations were further validated with measurable increases in functional plasticity (i.e., enhanced LTP in acute hippocampal slices) and synaptic proteins associated with functional plasticity as demonstrated by enhanced MLR-localization of NMDAR subunits (GluN1, GluN2A, and GluN2B). These ultrastructural alterations combined with the measurable electrophysiological changes in the hippocampus provide a mechanistic framework for the improved learning and memory dependent on the hippocampus observed in mice that similarly received *SynCav1* in the hippocampus (Mandyam et al. 2017). In summary, the ability of neuron-targeted Cav-1 to significantly augment synaptic plasticity in the hippocampus in vivo suggests that Cav-1 may be an attractive molecular target to improve brain function in the context of neurodegenerative diseases

Materials and Methods

Animals

All mice (C57BL/6) were treated in compliance with the Guide for the Care and Use of Laboratory Animals (National Academy of Science, Washington, DC). All animal use protocols were approved by the Veterans Administration San Diego Healthcare System Institutional Animal Care and Use Committee (IACUC, San Diego, CA) prior to procedures performed.

Stereotactic Injection

Adeno-associated viral (AAV) vectors were injected as previously described (Mandyam et al. 2017). Mice were anesthetized with 5% isoflurane mixed with 30% O_2, balanced with N_2 and then mounted onto a stereotaxic frame (Kopf; Berlin, Germany). Anesthesia was maintained with 1.4% isoflurane throughout the procedure. Hair was removed from top of head and the skin was cleansed. A dorsal skin incision was made to expose the skull. Skin was retracted and bilateral burr holes (5 mm diameter: 4 mm lateral, 0 mm rostral and 5 mm caudal to bregma) were made using a V35 electric hand piece (Buffalo Dental) as previously described (Niesman et al. 2014). The dura was carefully incised and a stereotaxic needle, attached to a precision micromanipulator (Neurostar), was positioned directly on top of the bregma. Hippocampal-targeted injections were controlled using Injectomate software (Neurostar). Injections were made using a 33 gauge 10 µL Hamilton Gas Tight syringe. At each coordinate, the needle was lowered at a rate of 0.32 mm/s. After 60 s, 0.5 µL of AAV serotype 9 (AAV9) containing synapsin-red fluorescent protein (*SynRFP*) or synapsin caveolin-1 (*SynCav1*) was injected over 30 s (1 µL/min injection rate) at 6 locations within the dorsal and ventral hippocampus along the anterior and posterior axis in each hemisphere with an indwelling time of 2 min (3 µL of total viral vector per hemisphere) to prevent reflux of vector solution. Viral *titer* = 10^9 viral particle/µL.

Electrophysiology

Hippocampal slices were prepared as previously described (Kleschevnikov et al. 2012). In short, mice were anesthetized with isoflurane before decapitation. The brain was quickly removed and

immersed for 2 min in ice-cold low-calcium "modified" artificial cerebrospinal fluid (mACSF) composed of (in mM): 119 NaCl, 2.5 KCl, 1.3 $CaCl_2$, 2.7 $MgSO_4$, 1 NaH_2PO_4, 26 $NaHCO_3$, and 10 glucose, osmolarity ~305 mOsm, continuously bubbled with 95% O_2–5% CO_2, pH 7.4. The dorsal hippocampus was dissected out and cut in ice-cold mACSF with a vibratome (Leica VT1000S; Nussloch) into 350 μm-thick slices from the middle part of the hippocampus. The slices were allowed to recover in oxygenated mACSF at 33 °C for 20 min, and then at room temperature for an additional 1.5–5 h before experimental recordings. Slices were transferred into the recording chamber and superfused with regular ACSF containing (in mM): 119 NaCl, 2.5 KCl, 2.5 $CaCl_2$, 1.3 $MgSO_4$, 1 NaH_2PO_4, 26 $NaHCO_3$, and 10 glucose, continuously bubbled with 95% O_2–5% CO_2, pH 7.4, osmolarity ~305 mOsm, at a constant rate of 2.5 mL/min at 32 °C. Recording electrodes were made of borosilicate glass capillaries (1B150F, World Precision Instruments) using a Sutter P-87 electrode puller (Sutter Instruments) and filled with ACSF (resistance ~0.8–1 MΩ). Monopolar stimulating electrodes were made of Pt/Ir (Platinum/Iridium) wires of diameter 25.4 μm (PTT0110, World Precision Instruments) with 100-μm-long exposed tips. Both the stimulating and recording electrodes were inserted under visual control perpendicular to the slice surface into the CA1 "stratum radiatum" at a distance 250–300 μm from each other. The initial slope of field excitatory postsynaptic potentials (fEPSPs) was measured at latencies 0.1–0.9 ms. Testing stimuli (duration 100 μs, current 70 μA) evoked field responses with amplitudes of 70–80% of maximum. After stabilization of responses, input–output dependences were measured using series of stimulation intensities (range 10–150 μA). LTP was induced by high-frequency tetanization (70 μA, 100 Hz for 1 sec) and was recorded 70 min after tetanus.

Biochemical Characterization of MLRs

Hippocampal tissue (50–100 mg) was homogenized using a carbonate lysis buffer (500 mM sodium carbonate, pH 11.0) containing protease and phosphatase inhibitors (Head et al. 2010). Lysates were sonicated on ice 3 times for 15 s each. Protein was quantified by Bradford assay and normalized to 0.5 mg/mL. Sucrose was dissolved in MBS (25 mM MES and 150 mM NaCl, pH 6.5) buffer to prepare 80%, 35%, and 5% solutions (Head et al. 2010). Sucrose gradients were prepared by adding 1 mL of 80% sucrose followed by 1 mL of sonicated sample with brief vortexing followed by 6 mL of 35% sucrose followed by 4 mL of 5% sucrose. Gradients were spun in an ultracentrifuge using a SW-41 rotor at 39k rpm at 4 °C for 3 h. Fractions (1 mL) were collected from the top of each tube starting at 4 to 12 mL. Samples were run as individual fractions 4–12 (buoyant fractions 4 and 5; BFs) for immunoblot analysis. Samples were run on 10% or 4–12% bis–tris gels (Life Technologies). After transfer to PDVF membranes, samples were incubated overnight with primary antibodies for Cav-1 (Cell Signaling #3238, 1:1000), GluN1A (Cell Signaling #5704, 1:1000), GluN2A (Cell Signaling #4207, 1:1000), or GluN2B (Cell Signaling #4205, 1:1000), and incubated with species-specific secondary antibodies conjugated to HRP. Densitometric analysis (arbitrary units) was conducted as previously described (Mandyam et al. 2017).

Electron Microscopy

For routine electron microscopy (EM) analysis (Figs 1–3), the brains were fixed with 2% glutaraldehyde, treated with 1% OsO_4, and were *en bloc* stained with uranyl acetate. For flat embedding of the sections, thin flexible molds were employed to lay the sections as level as possible in LX112 embedding media and then overlayed with plastic coverslips. The flat embedded blocks were visually trimmed to CA1 regions encompassing distal apical dendrites in the "stratum radiatum" of the hippocampus and thin sectioned to 70 nm. Grids were viewed unstained using FEI Tecnai EM scope. Excitatory or type I glutamatergic synapses were identified by the presence of a prominent, asymmetric postsynaptic density (PSD; Harris and Weinberg 2012); total synapses were normalized to the micrograph field (4800× magnification) as indicated in the Y-axis. PSVs were counted normalized to the total boutons per field as shown in Supplemental Fig. 1. G-ratio is defined as the diameter of the axon lumen divided by the diameter of the fiber (axon lumen plus myelin) (Pusic et al. 2016).

Immunogold EM

For immunogold EM, mouse brains were fixed for 12 h in 4% PFA in 0.1 M phosphate buffer, pelleted in 10% gelatin and cryoprotected in 2.3 M sucrose/phosphate buffer overnight at 4 °C. Blocks (1 mm^3) were mounted onto specimen holders and snap frozen in liquid nitrogen. Ultracryomicrotomy was carried out at –100 °C on a Leica Ultracut UCT with EM FCS cryoattachment (Leica) using a Diatome diamond knife (Diatome US, Hatfield, PA). 70 to 80 nm frozen sections were picked up with a 1:1 mixture of 2.3 M sucrose and 2% methyl cellulose (15cp) as described by Liou et al. (1996), and transferred onto Formvar and carbon-coated copper grids. For immunogold labeling, previously titrated primary antibodies (chicken anti-Cav-1, 1:100, a generous gift from Dr Radu V. Stan, Dartmouth Medical School), mouse antisynaptophysin (Biolegend #837 101, 1:100), rabbit antisynapsin (Cell Signaling #5297, 1:100), and mouse antitropomyosin receptor kinase B (TrkB, BD Transduction Labs #610 102, 1:10) were diluted in 1% BSA/PBS. Incubation with primary antibodies for 2 h at room temperature was followed by gold conjugated goat antimouse IgG & IgM (Jackson ImmunoResearch) or gold conjugated goat antirabbit IgG (or any other combination of secondary that was used with the gold particle size too), both diluted 1:25 in 1% BSA/PBS at room temperature for 45 minutes. Grids were then contrasted (10 min in 0.4% uranyl acetate and 1.8% methyl cellulose on ice) and viewed using a JEOL 1200EX II (JEOL, Peabody, MA) transmission electron microscope and photographed using a Gatan digital camera (Gatan), or viewed using a Tecnai G^2 Spirit BioTWIN transmission electron microscope equipped with an Eagle 4k HS digital camera (FEI). Quantitation was conducted in PhotoShop and analyzed with Prism 6.

Statistics

Normality of distribution tests were performed on data sets to determine parametric versus nonparametric statistical analyses. Data were then analyzed with two-way repeated measure analysis of variance (ANOVA) or Student's *t*-test. Post hoc tests were performed as appropriate. For the analyses, we used IBM SPSS v22 and Prism 6. Data are presented as mean ± SEM. Significance was assumed when $P < 0.05$. All experiments were double blinded to the experimenter (viral vector deliverer, electrophysiologist and microscopist).

Results

SynCav1 Promotes Ultrastructural Changes Indicative of Synaptic Plasticity

We previously demonstrated that *SynCav1* promotes dendritic arborization of hippocampal neurons and improves hippocampal-

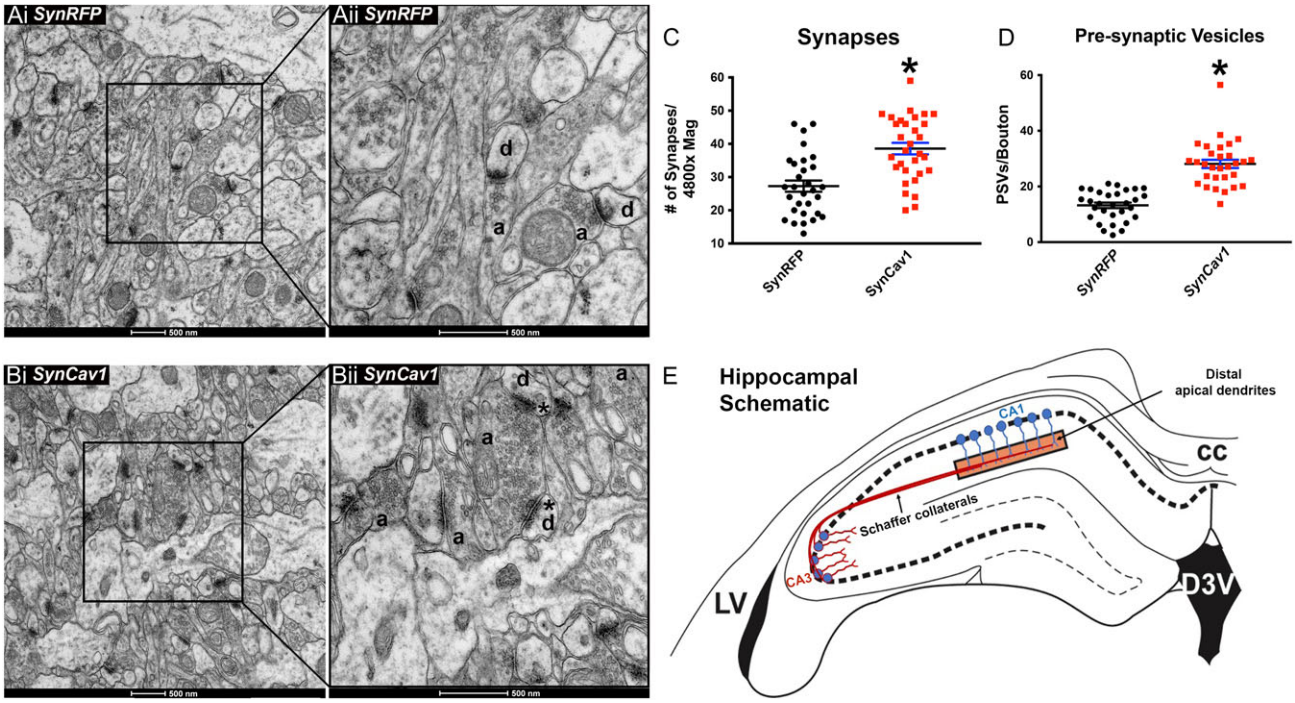

Figure 1. *SynCav1* increases total number of synapses and PSVs in the hippocampus. *AAV9-SynRFP* or *AAV9-SynCav1* was delivered to the hippocampus using stereotaxis, and 2 months later brains were prepared for routine EM. Hippocampal CA1 distal apical dendrites in the "stratum radiatum" were examined for ultrastructural changes using EM. (*Ai*,*ii*) *SynRFP*-injected mice; (*Bi*,*ii*) *SynCav1*-injected mice. a, axons; d, dendritic spines; asterisks indicate multiple-synapse boutons as previously described (Geinisman 1993; Fiala et al. 2002). Quantification of total synapses (*C*) and PSVs/axonal bouton (*D*). "Left panels" (9300× Mag); "right panels" (13 000× Mag of inset in "left panels"). (*$P < 0.05$, $n = 3$/group). Scale bar = 500 nm. (*E*) Hippocampal schematic illustrating the CA1 dendritic region (orange rectangle) used for EM imaging.

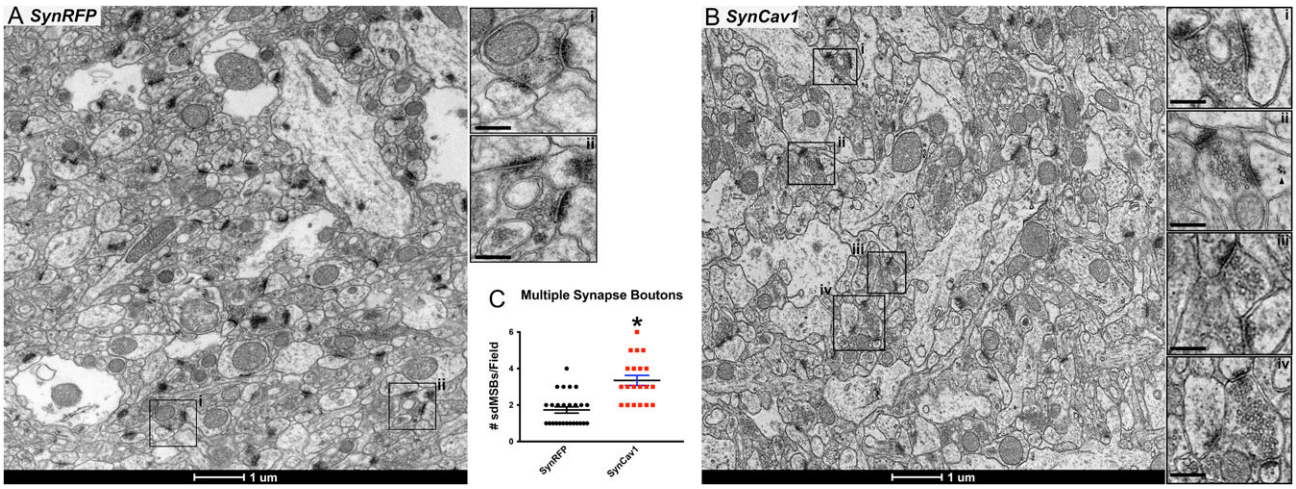

Figure 2. *SynCav1* increases total number of dsMBSs in the hippocampus. *AAV9-SynRFP* or *AAV9-SynCav1* was delivered directly to the hippocampus using stereotaxis, and 2 months later brains were prepared for routine EM. CA1 apical region in the hippocampus was examined for ultrastructural changes. (*A*) *SynRFP*-injected mice; examples of sdMSBs (Geinisman 1993; Fiala et al. 2002) are shown in insets i and ii. (*B*) *SynCav1*-injected mice; examples of sdMSBs are shown in insets i–iv; arrow head in Bii indicates polyribosome. "Left panels" (4800× Mag); "insets" (2.5× of 4800× image). (*C*) Quantification of *A* and *B* (*$P < 0.05$, $n = 3$/group). Scale bar = 1 μm; inset scale bar = 0.25 μm.

dependent learning and memory (Mandyam et al. 2017). We therefore performed EM on the hippocampus of *SynCav1*-injected adult mice to assess ultrastructural indicators of synaptic plasticity. Compared with mice that received *SynRFP*, *SynCav1* significantly increased total excitatory synapses with prominent asymmetric postsynaptic synaptic densities (Fig. 1A, $t(59) = 4.66$; $P < 0.0001$; *t*-test; and shown in Supplemental Fig. 1A), number of PSVs per axonal bouton (Fig. 1B, $t(58) = 8.31$; $P < 0.001$; *t*-test), and the number of dsMSBs (Fig. 2, $t(44) = 5.23$; $P < 0.0001$; *t*-test). We also used the G-ratio analysis (Pusic et al. 2016) to measure changes in myelination and found that *SynCav1* significantly lowered the G-ratio (Fig. 3A, $t(66) = 3.77$; $P = 0.0003$; *t*-test). This decreased G-ratio was not from the narrowing of the axon lumen (Fig. 3B, $t(64) = 0.44$; $P = 0.66$; *t*-test), but rather from an increased myelin diameter (Fig. 3C, $t(64) = 3.68$; $P = 0.0005$; *t*-test). These results demonstrate that *SynCav1* influences ultrastructural changes in the hippocampal CA1

subfield (composed of axons synapsing onto apical dendrites) consistent with those observed following events that promote synaptic plasticity (Geinisman 1993; Spacek and Harris 1997; Cooney et al. 2002; Ostroff et al. 2002).

Immunogold EM Shows that Cav-1 Localizes to Pre- and Postsynaptic Regions

To assess subsynaptic localization of Cav-1, we performed immunogold EM on asymmetric excitatory synapses located on distal apical dendrites in the hippocampal CA1 subfield. Compared with mice that received *SynRFP* (Fig. 4A), *SynCav1* (Fig. 4B) significantly increased the total Cav-1 immunogold particles in the PS region (Fig. 4C, $t(28) = 3.32$; $^{**}P = 0.0025$; *t*-test) and postsynaptic region (Fig. 4D. $t(29) = 2.76$; $^{*}P = 0.01$; *t*-test). Distribution analysis (Zhang et al. 2016) revealed that *SynCav1* significantly increased Cav-1 immungold particles proximal to pre- (effect of *SynCav1*: $F(6, 182) = 2.93$, $P = 0.009$; by two-way ANOVA, Fig. 4E) and postsynaptic membranes (effect of *SynCav1*: $F(6, 161) = 3.76$, $P = 0.002$; by two-way ANOVA, Fig. 4F). Post hoc test revealed a significant increase in Cav-1 immunogold particles within 50 nm of the PS ($^{***}P = 0.0001$; $^{*}P = 0.02$) and postsynaptic membrane ($^{****}P < 0.0001$; $^{**}P = 0.002$). Morphometric analysis revealed that *SynCav1* significantly increased PSD length (Fig. 4G, $t(41) = 2.98$; $^{**}P = 0.005$; *t*-test), width (Fig. 4H, $t(42) = 2.32$; $^{*}P = 0.035$; *t*-test), area (Fig. 4I, $t(41) = 3.33$; $^{**}P = 0.002$; *t*-test), and perimeter (Fig. 4J, $t(41) = 3.14$; $^{**}P = 0.003$; *t*-test). These results demonstrate that *SynCav1* increases Cav-1 localization to pre- and postsynaptic regions of excitatory

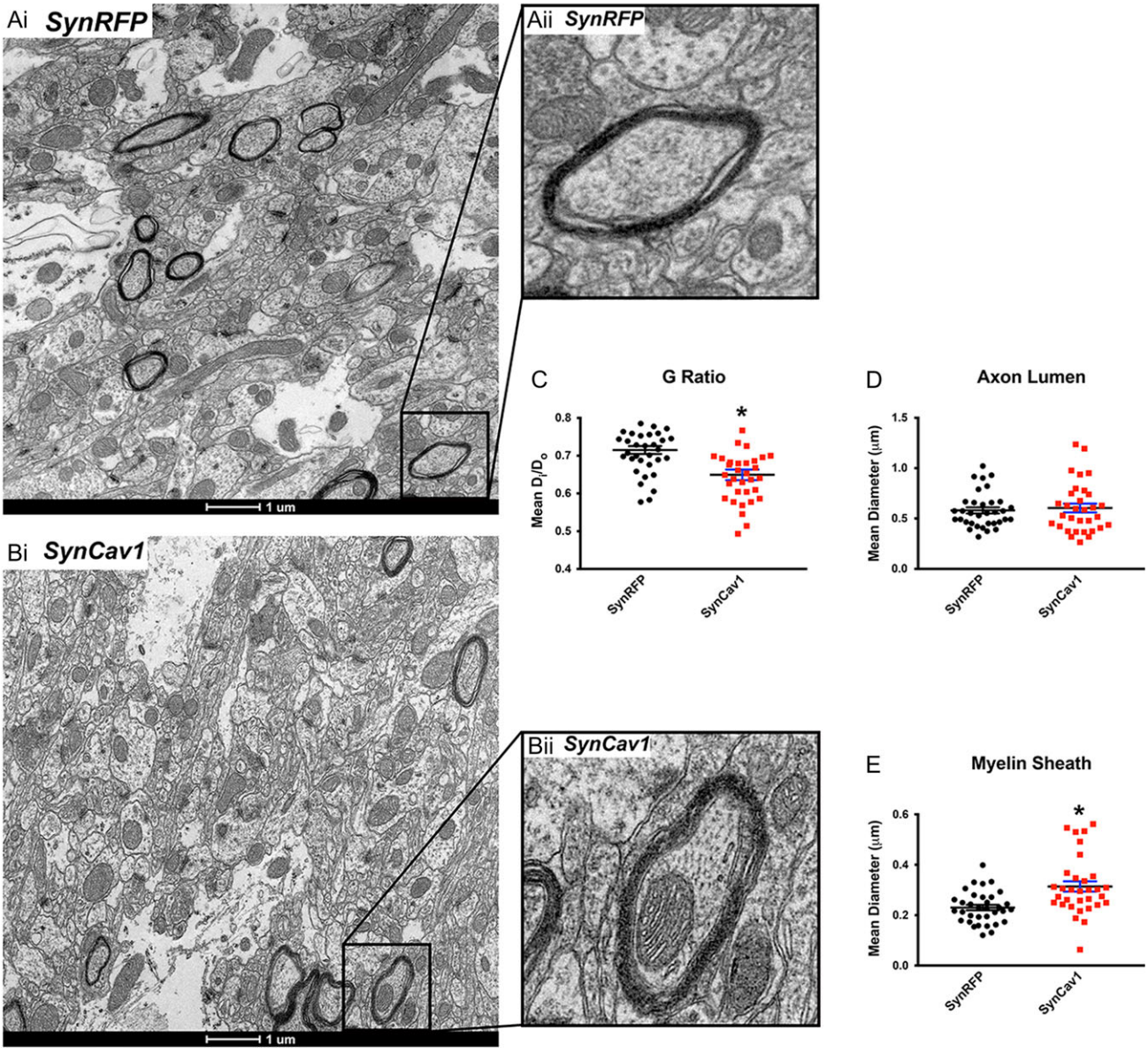

Figure 3. *SynCav1* increases myelin structure in the hippocampus. *AAV9-SynRFP* or *AAV9-SynCav1* was delivered directly to the hippocampus using stereotaxis, and 2 months later brains were prepared for routine EM. G-ratio analysis (axon lumen diameter/fiber diameter) was used to measure changes in myelination in Schaffer axons innervating the CA1 apical dendritic arbor in the hippocampus. (*Ai*) 4800× Mag of *SynRFP*-injected mice; (*Aii*) 3.5× magnification of the inset shown in (*Ai*). (*Bi*) 4800× Mag of *SynCav1*-injected mice; (*Bii*) 3.5× magnification of the inset shown in (*Bi*). Quantification of G-ratio (*C*), axonal lumen diameter (*D*), and myelin sheath diameter (*E*) was conducted using Adobe Photoshop ($^{*}P < 0.05$, $n = 3$/group). Scale bar = 1 μm.

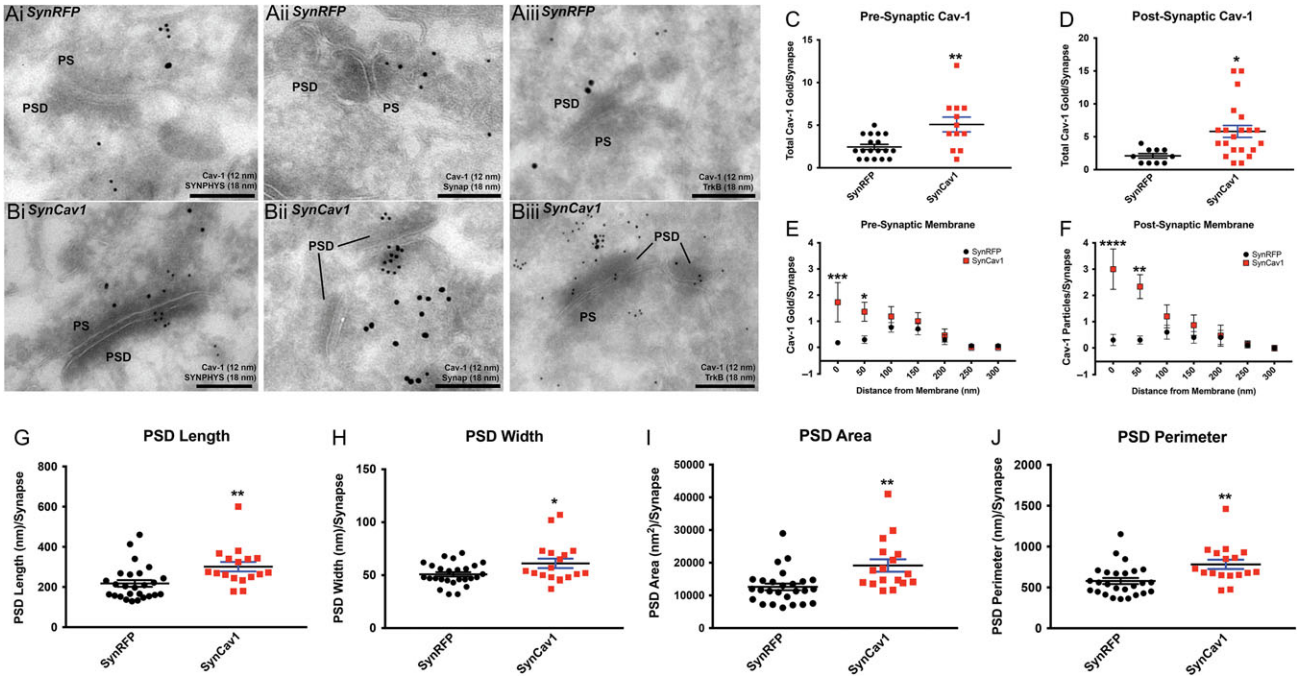

Figure 4. Immunogold EM showing Cav-1 subsynaptic localization at excitatory asymmetric synapses on distal apical CA1 dendrites. *AAV9-SynCav1* (or *AAV9-SynRFP*) was delivered to the hippocampus using stereotaxis, and 2 months later brains were prepared for immunogold EM. Hippocampal CA1 distal apical dendrites in the "stratum radiatum" were examined for subsynaptic localization of Cav-1 (12 nm gold) along with the PS markers SYNPHYS (18 nm gold) and Synap (18 nm) or the postsynaptic receptor TrkB (18 nm gold). Immunogold EM images are show in (*Ai–iii*) *SynRFP* and in (*Bi–iii*) *SynCav1*. Quantitation of total Cav-1 immunogold particles in PS (*C*) and postsynaptic (*D*) regions normalized per synapse. Distribution of Cav-1 immunogold particles relative to PS (*E*) and postsynaptic (*F*) membranes normalized per synapse. Morphometric analysis for PSD length (*G*), width (*H*), area (*I*), and perimeter (*J*). Data (mean ± SEM) were normalized to synapse as indicated in Y-axis (****$P < 0.0001$; ***$P = 0.0001$; **$P = 0.002$; *$P = 0.02$). Scale bar = 200 nm.

asymmetric synapses on CA1 distal apical dendrites with a corresponding increase in PSD size.

SynCav1 Enhances Hippocampal LTP in CA1 Neurons in the Hippocampus in Adult Mice

To assess synaptic properties, synaptic efficiency and plasticity (functional changes) in hippocampal neurons produced by *SynCav1* overexpression, we performed electrophysiological recordings in the hippocampal slices of mice injected with *SynCav1* or *SynRFP* (gene delivery at 4 months followed by euthanasia for brain measures at 6 months). First, the input–output dependence of fEPSPs, evoked by stimulation of the commissural-collateral input in the CA1, was examined. For all stimulating currents, evoked responses were statistically similar in both groups of mice suggesting that injections of *SynCav1* had no effect on baseline synaptic efficiency (Fig. 5A). To assess long-term synaptic plasticity, LTP in the CA1 region was examined by measuring fEPSP after CA3 Schaffer collateral stimulation. LTP was significantly greater in slices from *SynCav1* versus *SynRFP*-injected mice (effect of *SynCav1*: $F(87, 1408) = 1.413$, $P = 0.009$, $n = 8$–10 slices; by two-way ANOVA, Fig. 5B). Figure 5C represents mean ± SEM of data in Fig. 5B (*RFP* vs *Cav1*: 118.7 ± 4.02 *vs* 130.2 ± 4.44, $t(16) = 1.91$, $P = 0.037$). Interestingly, the difference in responses was observed immediately after the tetanization, suggesting that increased intrahippocampal levels of Cav-1 may affect induction of LTP. Thus, *SynCav1* promotes electrophysiological indicators of the Hebbian form of synaptic plasticity (Hebb 1949; Andersen et al. 2007), an event which requires activation of GluN receptor subunits.

SynCav1 Significantly Enhances NMDAR Subunits Localization to Hippocampal MLR Fractions

LTP and synaptic plasticity are dependent upon NMDAR function (Andersen et al. 2007). Considerable evidence shows that functional NMDAR localize to MLRs in neuronal membranes (Schrattenholz and Soskic 2006; Delint-Ramirez et al. 2008, 2010; Head et al. 2010). Because *SynCav1* promotes LTP as well as ultrastructural indicators of synaptic plasticity (i.e., increases synapses, PSVs/bouton, and multiple-synapse boutons), we assessed in our current model of synaptic plasticity whether *SynCav1* altered NMDAR expression. *SynCav1* increased total Cav-1 expression ($t(8) = 2.80$, $P = 0.02$) in hippocampal (Hpc) homogenates (Fig. 6A, B). Although no significant difference was detected in NMDAR subtype expression in Hpc homogenates (Fig. 6A, B), there was a significant increase in expression of GluN1A ($t(6) = 3.54$, $P = 0.01$), GluN2A ($t(6) = 2.77$, $P = 0.03$), GluN2B ($t(6) = 4.90$, $P = 0.003$), and Cav-1 ($t(8) = 2.67$, $P = 0.03$) in MLR fractions isolated from hippocampi of *SynCav1*-transfected mice (Fig. 6C, D), indicating altered subcellular localization.

Discussion

We have previously demonstrated that *SynCav1* overexpression in the hippocampus improves learning and memory dependent on the hippocampus (Mandyam et al. 2017). The present study extends this work and provides a molecular mechanistic framework by which *SynCav1* overexpression in the hippocampus increases total hippocampal synapses, density of PSVs per axonal bouton, and multiple-synapse boutons, all of which support synaptic plasticity at an ultrastructural level. These

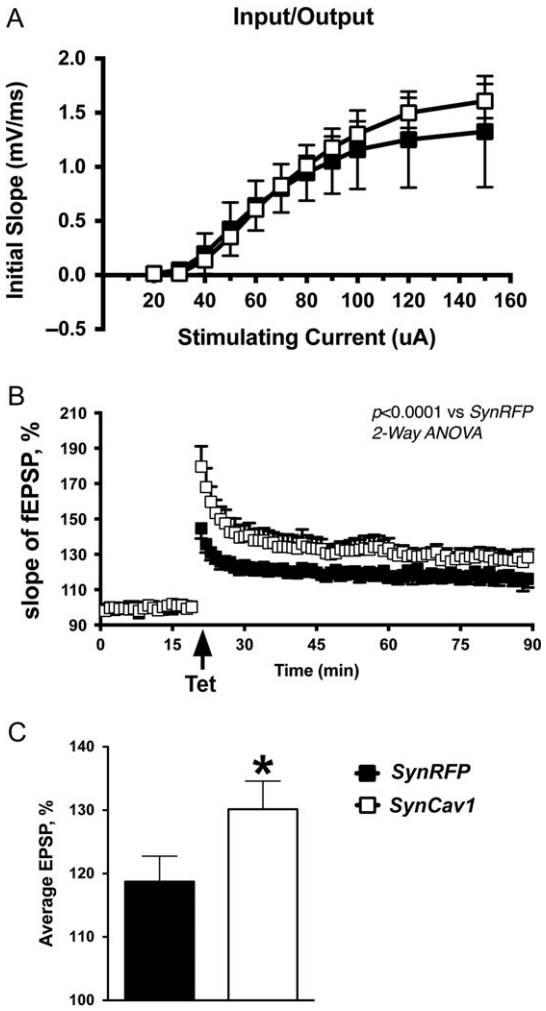

Figure 5. Effects of *SynCav1* and *SynRFP* on electrophysiological properties of the Schaffer collateral/CA1 synaptic pathway. (*A*) Input–output dependencies were similar in hippocampal slices prepared from AAV9-*SynCav1* and AAV9-*SynRFP*-treated mice. (*B*) LTP recording of field responses in the CA1 was measured over time following tetanization of the CA3 Schaffer collaterals. Tetanizations of afferent fibers (Tet, arrow) resulted in robust and stable increases of the evoked responses in both *SynCav1* and *SynRFP* mice. Note that the responses were greater in the *SynCav1*-injected mice. (*C*) Mean values of LTP shown in (*B*) (*$P < 0.05$, n = 8–10/group). LTP values shown in C represents averages taken 50–70 min after tetanus.

structural indicators of synaptic plasticity were further supported by electrophysiological (increases in LTP) and biochemical/subcellular (increased MLR-localization of NMDAR subunits) indicators of synaptic plasticity. Furthermore, this is the first study to demonstrate through high resolution immunogold EM that Cav-1 localizes to the PS axon terminal, in the synaptic cleft, and on the PSD of excitatory synapses on hippocampal CA1 apical dendrites. These findings indicate that Cav-1 in the adult hippocampus promotes structural and functional plasticity vital for hippocampal-dependent memory, and novel therapeutic strategies that augment Cav-1 expression specifically in neurons could be harnessed for its functional significance in neurodegenerative disorders.

Synaptic transmission occurs when NT are released from the PS membrane and activate postsynaptic membrane-localized receptors. Necessary for transmission are synaptic proteins that regulate (1) the reserve pool of PSVs, (2) mobilization and docking of PSVs to the PS membrane, (3) membrane fusion and Ca^{2+}-triggered NT release, and (4) vesicle endocytosis, recycling, and refilling (Rizo and Sudhof 2002; Andersen et al. 2007). PSVs are tethered to actin by synapsin (Synap) proteins within 200–500 nm of PS membrane (i.e., active zone) (Andersen et al. 2007). Kinases such as protein kinase A and calcium/calmodulin-dependent protein kinase II (CaMKII) directly or indirectly lead to Synap phosphorylation, respectively, allowing for PSV release and mobilization to the active zone (Chi et al. 2003; Menegon et al. 2006). At the membrane, vesicular (v-)SNARE proteins on the vesicular membrane (e.g., SYNPHYS) bind target (t-)SNARES (e.g., SNAP25 and syntaxin) on the active zone membrane resulting in membrane fusion and NT release. Membrane cholesterol enhances the negative curvature of plasma membrane, thus increasing the fusogenecity of the PSV with the cytofacial leaflet of the membrane (Egawa et al. 2016). Interestingly, much evidence shows that SNARE complexes localize to cholesterol-enriched MLRs in neurons (Chamberlain et al. 2001; Lang et al. 2001; Chamberlain and Gould 2002; Egawa et al. 2016). We have previously shown that *SynCav1* increases membrane cholesterol, MLR formation, GluN receptor-mediated CaMKII phosphorylation, and expression of SNARE proteins (e.g., synaptobrevin and syntaxin) in neurons in vitro (rodent and human) (Head et al. 2011; Kassan et al. 2017). Moreover, *SynCav1* delivery to mice in vivo increases hippocampal expression of SNARE proteins (synaptobrevin, syntaxin) (Kassan et al. 2017). Although not measured in the current study, these previous findings may in part explain the mechanisms underlying increased density of PSVs and overall increase in total hippocampal synapses reported in the current study.

Neurons are highly polarized cells with long axons and dendritic arbors that enable interneuronal communication. Formation/maintenance of these intercellular connections requires proper subcellular localization of signaling components, such as NMDAR, a NT receptor critical for LTP; NMDARs localize to neuronal MLRs (Schrattenholz and Soskic 2006; Delint-Ramirez et al. 2008, 2010; Head et al. 2010). Interestingly, MLRs and synapses are composed of identical biophysical and chemical properties (e.g., cholesterol, sphingolipids, similar proteins) and are now considered one and the same (Liu et al. 2013; Madwar et al. 2016). Depletion of cholesterol disrupts MLRs and impairs NMDAR-mediated signaling and LTP (Frank et al. 2008; Korinek et al. 2015). LTP alone increases cholesterol synthesis, and much evidence suggests that LTP-mediated plasticity may in part depend upon cholesterol (Egawa et al. 2016). Previous in vitro work showing *SynCav1* increases MLRs and NMDAR-mediated signaling (P-CaMKII) (Head et al. 2011) is further extended by the present biochemical and eletrophysiological findings that *SynCav1* increases MLR-localized NMDARs and augments LTP, suggesting a possible molecular mechanism underlying the *SynCav1*-mediated ultrastructural changes as measured by EM (Figs 1 and 2). How MLR and Cav-1 (and possibly cholesterol) recruit and modulate NMDAR function in MLRs requires further investigation.

Myelin is a multilaminar sheath which insulates axons and speeds up conductance velocity (Lussier and Rushton 1951; Rushton 1951). Myelin structure is positively modified by experience, information processing, learning and memory (Fields 2008). G-ratio (axon diameter divided by fiber diameter), a reliable measure of axonal myelination (Rushton 1951; Chomiak and Hu 2009), was significantly lowered with *SynCav1*. *SynCav1*-mediated decrease in G-ratio (0.72 in *SynRFP* mice vs. 0.65 in *SynCav1* mice) was comparable to that measured in the rodent CNS following exposure to an enriched environment (EE) (G-ratio

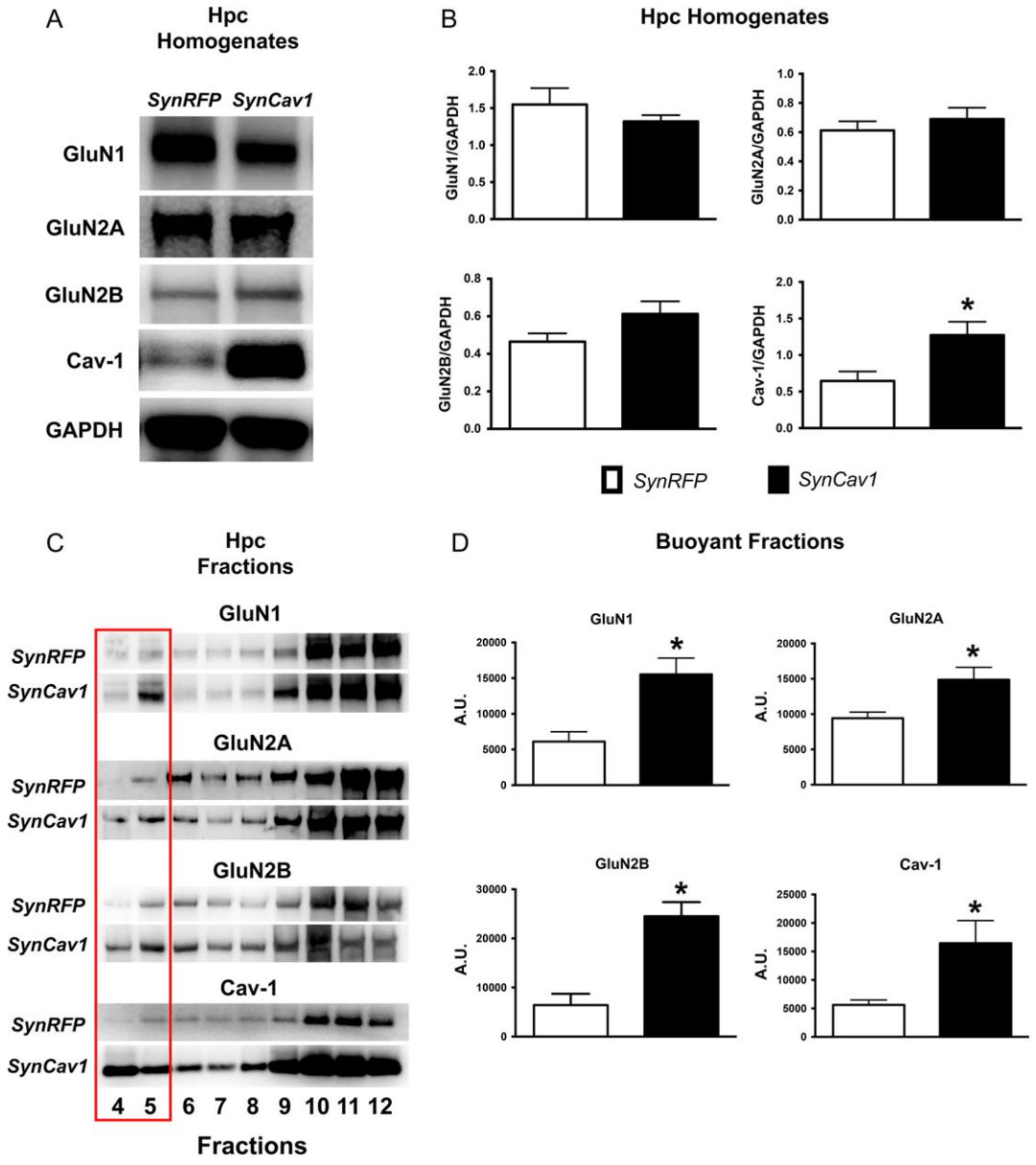

Figure 6. *SynCav1* significantly enhances MLR-localization of NMDAR subunits in adult hippocampus. (*A*) Hippocampal (Hpc) homogenates from *AAV9-SynCav1* and *AAV9-SynRFP*-treated mice were immunobloted for NMDAR subunits GluN1A, GluN2A, GluN2B, and Cav-1. Quantitation (normalized to GAPDH) is shown in (*B*). (*C*) Hpc homogenates (equal protein loading of 0.5 mg/mL) were subjected to sucrose density fraction (BFs) followed by immunoblot analysis. Quantitation is shown in (*D*). Red box demarcates MLR fractions 4 and 5 (BF). Data represent arbitrary units (A.U.) mean ± SEM (*$P < 0.05$, $n = 4$/group).

decline from 0.77 to 0.69 following EE in Pusic et al. (2016)). These findings have potential implications for neurodegenerative diseases that exhibit altered myelin structure such as multiple sclerosis (MS), amyotrophic lateral sclerosis, Alzheimer's disease (AD), and even in psychiatric disorders like schizophrenia, depression, ADHD, PTSD, and obsessive-compulsive disorder, which all show signs of altered myelin structure (i.e., decreased white matter) (Fields 2008). Altered myelin structure can disrupt cognition in individuals with MS, and aged-related cognitive decline correlates with altered myelin structure (Kujala et al. 1997; Gootjes et al. 2004). Conversely, increased myelin correlates with higher cognitive function, learning and memory, and higher intelligent quotient. Moreover, increased myelination of certain brain regions positively correlates with reading ability (Kraft et al. 1980), vocabulary learning (Pujol et al. 2006), executive decision making (Giedd 2004; Liston et al. 2006), and complex skills such as learning a musical instrument (Bengtsson et al. 2005). The present study demonstrating *SynCav1* increases myelination may in part explain previous work showing improved learning and memory in *SynCav1*-treated mice (Mandyam et al. 2017). Myelin structure is dynamic, regulated by impulse activity, and changes with functional experience and is suggested to be an additional form of "plasticity" that works in concert with synaptic plasticity (Laurenzana et al. 2015). One caveat is that the vector we used is neuron specific (i.e., Synap-driven Cav-1 expression), and therefore it is not precisely clear why there would be increased myelin. Are higher functioning neurons requiring more myelin? Or are *SynCav1*-treated neurons releasing factors (such as exosomes) that activate myelinating oligodendrocytes (Pusic et al. 2016)? Further

investigation is required to elucidate how *SynCav1* increases myelination in the CNS.

Restoration of synaptic plasticity and cognitive function in the neurodegenerative brain remains a major medical challenge. Much evidence shows impaired synaptic function in neurodegenerative diseases such as AD. Pathological hippocampal specimens from AD individuals reveal a 60% decrease in the density of PS boutons as well as a reduction in synaptic vesicle markers when compared with control patients (Scheff et al. 1996). Preclinical studies using AD models reveal abnormalities in synaptic transmission, reduced CA1 dendritic EPSPs following Schaffer collateral stimulation (i.e., impaired LTP) (Larson et al. 1999; Giacchino et al. 2000). The neurodegenerative brain demonstrates impaired cognition, deficits in learning and memory (Leal and Yassa 2013; Fjell et al. 2014; Morrison and Baxter 2014), reduced number of synapses in the hippocampus (DG and CA1 subfield) and medial prefrontal cortex (Mesulam 1999; Fjell et al. 2014), decreased LTP (Chapman et al. 1999; Moechars et al. 1999; Rosenzweig and Barnes 2003; Small et al. 2011), and an inability to evoke neuroplasticity. Restoring or enhancing the molecular mechanistic framework necessary for synaptic transmission are attractive therapeutic targets for improving function in the neurodegenerative CNS.

One limitation to the present study is whether other receptors are involved in Cav-1-induced synaptic and neuroplasticity. Several receptors in addition to NMDARs such as AMPARs are also essential to hippocampal synaptic plasticity. The current study focused on NMDARs predominantly because previous in vitro work from our group has shown that Cav-1: (1) regulates NMDAR signaling and neuroprotection against oxygen glucose deprivation and (2) modulates NMDAR-localization to MLRs in primary neurons. NMDARs play a critical role in the induction of LTP, specifically in CA1 pyramidal neurons and hippocampal-dependent learning. NMDARs play a critical role in the induction of LTP and hippocampal-dependent learning. The cellular event that triggers LTP induction occurs through Ca^{2+} influx as a result of NMDAR activation, especially by Schaffer collateral synapses on CA1 pyramidal cells. Because we detected *SynCav1*-mediated LTP in the CA1 subfield (Fig. 5), we wanted to investigate whether also *SynCav1* altered the subcellular distribution and expression of NMDAR in the hippocampus in vivo similar to what we have measured with *SynCav1* in vitro (Head et al. 2008, 2011).

A second limitation to this study was that we did not identify the type of PSVs that aggregated at axon terminals shown in Figs 1 and 2. However, morphologically these synapses were asymmetric in that they exhibited electron-dense postsynaptic thickening, a hallmark of type I excitatory synapses (Andersen et al. 1966). Furthermore, these synapses were enriched in SYNPHYS immunogold particles on the PS side as shown in Figure 4 and were located on the CA1 apical dendritic arbor projecting into the "stratum radiatum", a brain region highly enriched in glutamatergic synapses (Harris and Stewart 2001). In addition, based upon the anatomical region mentioned above, the presence of myelinated axons is consistent with the Schaffer collateral commissural fibers originating from CA3 pyramidal neurons, one of the few myelinated axons in the entire hippocampus (in contrast to thinner, unmyelinated mossy fibers) (Ishizuka et al. 1990; Shepherd and Harris 1998; Shepherd et al. 2002). Moreover, this is the same hippocampal region (CA1) from which we recorded elevated LTP with *SynCav1*.

A third limitation to this study is our inability to distinguish among which neuronal subtypes expressed the transgene (i.e., primary neurons vs. interneurons or glutamatergic vs. serotonergic, dopaminergic, etc.). Although the vector contains a neuron-specific Synap promoter, it unfortunately does not allow one to distinguish among different neuronal cell populations. Previously, we observed augmented dopaminergic and serotonergic receptor signaling (in addition to glutamatergic signaling) with *SynCav1* in vitro (Head et al. 2011). However, these findings did not confirm specifically which neuronal subtype is directly expressing the Cav-1 transgene. Evidence from our published work in "Biological Psychiatry" demonstrate that the majority of the hippocampus exhibited global RFP expression after *AAV9-SynRFP* delivery to 3 hippocampal locations (rostral to caudal), suggesting multiple neuronal population subtypes expressed the Synap-driven transgene (Mandyam et al. 2017). The current findings provide strong evidence that neuron-targeted Cav-1 overexpression in the hippocampus resultants in ultrastructural, electrophysiological, and biochemical indicators of functional synaptic plasticity. Yet, whether these changes in the hippocampus occur solely from targeting primary cells only or also include interneurons still needs further investigation.

In conclusion, neuronal Cav-1 may serve as a protein in neuronal MLRs that "primes" the system for higher performance. Through scaffolding and localizing key synaptic proteins (SNAREs and PSD proteins), *SynCav1* may promote the molecular and subcellular events that augment functional synaptic transmission. Biophysically, Cav-1 with cholesterol may enhance the fusogenicity between PSVs and target PS membranes resulting in NT release. By influencing these subcellular events, *SynCav1* may strengthen existing synapses and promote formation of new functional synapses. The present study provides direct evidence that neuron-targeted Cav-1 promotes synaptic plasticity at an ultrastructural and subcellular level. A better understanding of how the molecular framework for synaptic plasticity is organized subcellularly will yield knowledge vital for generating novel strategies to combat neurodegenerative conditions.

Supplementary Material

Supplementary data are available at *Cerebral Cortex* online.

Funding

Work in the authors' laboratories is supported by Veterans Affairs Merit Award from the Department of Veterans Affairs BX003671 (B. P. Head), BX000783 (D. M. Roth), and BX001963 (H. H. Patel), National Institutes of Health, Bethesda, MD, U.S.A., NS073653 (B. P. Head); HL091071 and HL107200 (H. H. Patel); GM085179 (P. M. Patel); DA034140 and AA020098 (C. D. Mandyam); The Jerome Lejeune Foundation Grant (A.M. Kleschevnikov).

Notes

We want to thank Ying Jones, Vanessa Taupin, Timo Meerloo, and Dr Marilyn Farquhar at the UCSD EM core for preparation of the brain samples and training on the EM. We also want to thank Dr Radu V. Stan from Dartmouth Medical School for providing us with the chicken anti-Cav-1 primary antibody used for immunogold EM. We would also like to thank Matt Hunt for his consultation on performing G-ratio analysis using Adobe Photoshop. *Conflict of Interest*: None declared.

References

Abraham WC. 2003. How long will long-term potentiation last? Philos Trans R Soc Lond B Biol Sci. 358:735–744.

Andersen P. 1960. Interhippocampal impulses. II. Apical dendritic activation of CAI neurons. Acta Physiol Scand. 48: 178–208.

Andersen P, Blackstad TW, Lomo T. 1966. Location and identification of excitatory synapses on hippocampal pyramidal cells. Exp Brain Res. 1:236–248.

Andersen P, Morris R, Amaral D, Bliss T, O'Keefe J 2007. The Hippocampus Book. Oxford Neuroscience Series. New York: Oxford University Press.

Bengtsson SL, Nagy Z, Skare S, Forsman L, Forssberg H, Ullen F. 2005. Extensive piano practicing has regionally specific effects on white matter development. Nat Neurosci. 8: 1148–1150.

Bliss TV, Lomo T. 1973. Long-lasting potentiation of synaptic transmission in the dentate area of the anaesthetized rabbit following stimulation of the perforant path. J Physiol. 232: 331–356.

Bourne JN, Harris KM. 2011. Coordination of size and number of excitatory and inhibitory synapses results in a balanced structural plasticity along mature hippocampal CA1 dendrites during LTP. Hippocampus. 21:354–373.

Chamberlain LH, Burgoyne RD, Gould GW. 2001. SNARE proteins are highly enriched in lipid rafts in PC12 cells: implications for the spatial control of exocytosis. Proc Natl Acad Sci USA. 98:5619–5624.

Chamberlain LH, Gould GW. 2002. The vesicle- and target-SNARE proteins that mediate Glut4 vesicle fusion are localized in detergent-insoluble lipid rafts present on distinct intracellular membranes. J Biol Chem. 277:49750–49754.

Chapman PF, White GL, Jones MW, Cooper-Blacketer D, Marshall VJ, Irizarry M, Younkin L, Good MA, Bliss TV, Hyman BT, et al. 1999. Impaired synaptic plasticity and learning in aged amyloid precursor protein transgenic mice. Nat Neurosci. 2:271–276.

Chi P, Greengard P, Ryan TA. 2003. Synaptic vesicle mobilization is regulated by distinct synapsin I phosphorylation pathways at different frequencies. Neuron. 38:69–78.

Chomiak T, Hu B. 2009. What is the optimal value of the g-ratio for myelinated fibers in the rat CNS? A theoretical approach. PLoS One. 4:e7754.

Cooney JR, Hurlburt JL, Selig DK, Harris KM, Fiala JC. 2002. Endosomal compartments serve multiple hippocampal dendritic spines from a widespread rather than a local store of recycling membrane. J Neurosci. 22:2215–2224.

Da Silva JS, Hasegawa T, Miyagi T, Dotti CG, Abad-Rodriguez J. 2005. Asymmetric membrane ganglioside sialidase activity specifies axonal fate. Nat Neurosci. 8:606–615.

de Kreuk BJ, Nethe M, Fernandez-Borja M, Anthony EC, Hensbergen PJ, Deelder AM, Plomann M, Hordijk PL. 2011. The F-BAR domain protein PACSIN2 associates with Rac1 and regulates cell spreading and migration. J Cell Sci. 124: 2375–2388.

Del Pozo MA, Schwartz MA. 2007. Rac, membrane heterogeneity, caveolin and regulation of growth by integrins. Trends Cell Biol. 17:246–250.

Delint-Ramirez I, Fernandez E, Bayes A, Kicsi E, Komiyama NH, Grant SG. 2010. In vivo composition of NMDA receptor signaling complexes differs between membrane subdomains and is modulated by PSD-95 and PSD-93. J Neurosci. 30: 8162–8170.

Delint-Ramirez I, Salcedo-Tello P, Bermudez-Rattoni F. 2008. Spatial memory formation induces recruitment of NMDA receptor and PSD-95 to synaptic lipid rafts. J Neurochem. 106:1658–1668.

Denny JB. 2006. Molecular Mechanisms, Biological Actions, and Neuropharmacology of the Growth-Associated Protein GAP-43. Curr Neuropharmacol. 4:293–304.

Douglas RM, Goddard GV. 1975. Long-term potentiation of the perforant path-granule cell synapse in the rat hippocampus. Brain Res. 86:205–215.

Egawa J, Pearn ML, Lemkuil BP, Patel PM, Head BP. 2016. Membrane lipid rafts and neurobiology: age-related changes in membrane lipids and loss of neuronal function. J Physiol. 594:4565–4579.

Egawa J, Schilling JM, Cui W, Posadas E, Sawada A, Alas B, Zemljic-Harpf AE, Fannon-Pavlich MJ, Mandyam CD, Roth DM, et al. 2017. Neuron-specific caveolin-1 overexpression improves motor function and preserves memory in mice subjected to brain trauma. FASEB J. pii: fj.201601288RRR. doi: 10.1096/fj.201601288RRR.

Fiala JC, Allwardt B, Harris KM. 2002. Dendritic spines do not split during hippocampal LTP or maturation. Nat Neurosci. 5:297–298.

Fields RD. 2008. White matter in learning, cognition and psychiatric disorders. Trends Neurosci. 31:361–370.

Fjell AM, McEvoy L, Holland D, Dale AM, Walhovd KB, Alzheimer's Disease Neuroimaging I. 2014. What is normal in normal aging? Effects of aging, amyloid and Alzheimer's disease on the cerebral cortex and the hippocampus. Prog Neurobiol. 117C:20–40.

Frank C, Rufini S, Tancredi V, Forcina R, Grossi D, D'Arcangelo G. 2008. Cholesterol depletion inhibits synaptic transmission and synaptic plasticity in rat hippocampus. Exp Neurol. 212: 407–414.

Garcia-Martinez V, Montes MA, Villanueva J, Gimenez-Molina Y, de Toledo GA, Gutierrez LM. 2015. Sphingomyelin derivatives increase the frequency of microvesicle and granule fusion in chromaffin cells. Neuroscience. 295:117–125.

Geinisman Y. 1993. Perforated axospinous synapses with multiple, completely partitioned transmission zones: probable structural intermediates in synaptic plasticity. Hippocampus. 3:417–433.

Giacchino J, Criado JR, Games D, Henriksen S. 2000. In vivo synaptic transmission in young and aged amyloid precursor protein transgenic mice. Brain Res. 876:185–190.

Giedd JN. 2004. Structural magnetic resonance imaging of the adolescent brain. Ann N Y Acad Sci. 1021:77–85.

Gil C, Soler-Jover A, Blasi J, Aguilera J. 2005. Synaptic proteins and SNARE complexes are localized in lipid rafts from rat brain synaptosomes. Biochem Biophys Res Commun. 329:117–124.

Gootjes L, Teipel SJ, Zebuhr Y, Schwarz R, Leinsinger G, Scheltens P, Moller HJ, Hampel H. 2004. Regional distribution of white matter hyperintensities in vascular dementia, Alzheimer's disease and healthy aging. Dement Geriatr Cogn Disord. 18:180–188.

Grande-Garcia A, del Pozo MA. 2008. Caveolin-1 in cell polarization and directional migration. Eur J Cell Biol. 87:641–647.

Guirland C, Zheng JQ. 2007. Membrane lipid rafts and their role in axon guidance. Adv Exp Med Biol. 621:144–155.

Harris E, Stewart M. 2001. Intrinsic connectivity of the rat subiculum: II. Properties of synchronous spontaneous activity and a demonstration of multiple generator regions. J Comp Neurol. 435:506–518.

Harris KM, Weinberg RJ. 2012. Ultrastructure of synapses in the mammalian brain. Cold Spring Harb Perspect Biol. 4:1–30.

Head BP, Hu Y, Finley JC, Saldana MD, Bonds JA, Miyanohara A, Niesman IR, Ali SS, Murray F, Insel PA, et al. 2011. Neuron-targeted caveolin-1 protein enhances signaling and promotes arborization of primary neurons. J Biol Chem. 286: 33310–33321.

Head BP, Patel HH, Insel PA. 2014. Interaction of membrane/lipid rafts with the cytoskeleton: impact on signaling and function: Membrane/lipid rafts, mediators of cytoskeletal arrangement and cell signaling. Biochim Biophys Acta. 1838: 532–545.

Head BP, Patel HH, Roth DM, Murray F, Swaney JS, Niesman IR, Farquhar MG, Insel PA. 2006. Microtubules and actin microfilaments regulate lipid raft/caveolae localization of adenylyl cyclase signaling components. J Biol Chem. 281:26391–26399.

Head BP, Patel HH, Tsutsumi YM, Hu Y, Mejia T, Mora RC, Insel PA, Roth DM, Drummond JC, Patel PM. 2008. Caveolin-1 expression is essential for N-methyl-D-aspartate receptor-mediated Src and extracellular signal-regulated kinase 1/2 activation and protection of primary neurons from ischemic cell death. FASEB J. 22:828–840.

Head BP, Peart JN, Panneerselvam M, Yokoyama T, Pearn ML, Niesman IR, Bonds JA, Schilling JM, Miyanohara A, Headrick J, et al. 2010. Loss of caveolin-1 accelerates neurodegeneration and aging. PLoS One. 5:e15697.

Hebb DO. 1949. The Organziation of Behavior. New York: Wiley.

Ishizuka N, Weber J, Amaral DG. 1990. Organization of intrahippocampal projections originating from CA3 pyramidal cells in the rat. J Comp Neurol. 295:580–623.

Kamiguchi H. 2006. The region-specific activities of lipid rafts during axon growth and guidance. J Neurochem. 98:330–335.

Kassan A, Egawa J, Zhang Z, Almenar-Queralt A, Nguyen QM, Lajevardi Y, Kim K, Posadas E, Jeste DV, Roth DM, et al. 2017. Caveolin-1 regulation of disrupted-in-schizophrenia-1 as a potential therapeutic target for schizophrenia. J Neurophysiol. 117:436–444.

Kleschevnikov AM, Belichenko PV, Faizi M, Jacobs LF, Htun K, Shamloo M, Mobley WC. 2012. Deficits in cognition and synaptic plasticity in a mouse model of Down syndrome ameliorated by GABAB receptor antagonists. J Neurosci. 32: 9217–9227.

Konorski J. 1948. Conditioned Reflexes Nad Neuron Organziation. Cambridge: University Press. p. 267.

Korinek M, Vyklicky V, Borovska J, Lichnerova K, Kaniakova M, Krausova B, Krusek J, Balik A, Smejkalova T, Horak M, et al. 2015. Cholesterol modulates open probability and desensitization of NMDA receptors. J Physiol. 593:2279–2293.

Kraft RH, Mitchell OR, Languis ML, Wheatley GH. 1980. Hemispheric asymmetries during six- to eight-year-olds performance of Piagetian conservation and reading tasks. Neuropsychologia. 18:637–643.

Kujala P, Portin R, Ruutiainen J. 1997. The progress of cognitive decline in multiple sclerosis. A controlled 3-year follow-up. Brain. 120(Pt 2):289–297.

Lang T, Bruns D, Wenzel D, Riedel D, Holroyd P, Thiele C, Jahn R. 2001. SNAREs are concentrated in cholesterol-dependent clusters that define docking and fusion sites for exocytosis. EMBO J. 20:2202–2213.

Larson J, Lynch G, Games D, Seubert P. 1999. Alterations in synaptic transmission and long-term potentiation in hippocampal slices from young and aged PDAPP mice. Brain Res. 840:23–35.

Laurenzana A, Fibbi G, Chilla A, Margheri G, Del Rosso T, Rovida E, Del Rosso M, Margheri F. 2015. Lipid rafts: integrated platforms for vascular organization offering therapeutic opportunities. Cell Mol Life Sci. 72:1537–1557.

Leal SL, Yassa MA. 2013. Perturbations of neural circuitry in aging, mild cognitive impairment, and Alzheimer's disease. Ageing Res Rev. 12:823–831.

Liou W, Geuze HJ, Slot JW. 1996. Improving structural integrity of cryosections for immunogold labeling. Histochem Cell Biol. 106:41–58.

Liston C, Watts R, Tottenham N, Davidson MC, Niogi S, Ulug AM, Casey BJ. 2006. Frontostriatal microstructure modulates efficient recruitment of cognitive control. Cereb Cortex. 16: 553–560.

Liu Q, Yao WD, Suzuki T. 2013. Specific interaction of postsynaptic densities with membrane rafts isolated from synaptic plasma membranes. J Neurogenet. 27:43–58.

Lussier JJ, Rushton WA. 1951. Excitability of the nodes of Ranvier in a nerve trunk. J Physiol. 115:53.

Madwar C, Gopalakrishnan G, Lennox RB. 2016. Lipid microdomains in synapse formation. ACS Chem Neurosci. 7: 833–841.

Mandyam CD, Schilling JM, Cui W, Egawa J, Niesman IR, Kellerhals SE, Staples MC, Busija AR, Risbrough VB, Posadas E, et al. 2017. Neuron-targeted Caveolin-1 improves molecular signaling, plasticity, and behavior dependent on the hippocampus in adult and aged mice. Biol Psychiatry. 81: 101–110.

Menegon A, Bonanomi D, Albertinazzi C, Lotti F, Ferrari G, Kao HT, Benfenati F, Baldelli P, Valtorta F. 2006. Protein kinase A-mediated synapsin I phosphorylation is a central modulator of Ca2+-dependent synaptic activity. J Neurosci. 26:11670–11681.

Mesulam MM. 1999. Neuroplasticity failure in Alzheimer's disease: bridging the gap between plaques and tangles. Neuron. 24:521–529.

Moechars D, Dewachter I, Lorent K, Reverse D, Baekelandt V, Naidu A, Tesseur I, Spittaels K, Haute CV, Checler F, et al. 1999. Early phenotypic changes in transgenic mice that overexpress different mutants of amyloid precursor protein in brain. J Biol Chem. 274:6483–6492.

Morrison JH, Baxter MG. 2014. Synaptic health. JAMA psychiatry. 71:835–837.

Nakai Y, Kamiguchi H. 2002. Migration of nerve growth cones requires detergent-resistant membranes in a spatially defined and substrate-dependent manner. J Cell Biol. 159: 1097–1108.

Niesman IR, Schilling JM, Shapiro LA, Kellerhals SE, Bonds JA, Kleschevnikov AM, Cui W, Voong A, Krajewski S, Ali SS, et al. 2014. Traumatic brain injury enhances neuroinflammation and lesion volume in caveolin deficient mice. J Neuroinflammation. 11:39.

Niethammer P, Delling M, Sytnyk V, Dityatev A, Fukami K, Schachner M. 2002. Cosignaling of NCAM via lipid rafts and the FGF receptor is required for neuritogenesis. J Cell Biol. 157:521–532.

Ostroff LE, Fiala JC, Allwardt B, Harris KM. 2002. Polyribosomes redistribute from dendritic shafts into spines with enlarged synapses during LTP in developing rat hippocampal slices. Neuron. 35:535–545.

Pujol J, Soriano-Mas C, Ortiz H, Sebastian-Galles N, Losilla JM, Deus J. 2006. Myelination of language-related areas in the developing brain. Neurology. 66:339–343.

Pusic KM, Pusic AD, Kraig RP. 2016. Environmental enrichment stimulates immune cell secretion of exosomes that promote CNS myelination and may regulate inflammation. Cell Mol Neurobiol. 36:313–325.

Rizo J, Sudhof TC. 2002. Snares and Munc18 in synaptic vesicle fusion. Nat Rev Neurosci. 3:641–653.

Rosenzweig ES, Barnes CA. 2003. Impact of aging on hippocampal function: plasticity, network dynamics, and cognition. Prog Neurobiol. 69:143–179.

Rushton WA. 1951. A theory of the effects of fibre size in medullated nerve. J Physiol. 115:101–122.

Scheff SW, Sparks DL, Price DA. 1996. Quantitative assessment of synaptic density in the outer molecular layer of the hippocampal dentate gyrus in Alzheimer's disease. Dementia. 7:226–232.

Schrattenholz A, Soskic V. 2006. NMDA receptors are not alone: dynamic regulation of NMDA receptor structure and function by neuregulins and transient cholesterol-rich membrane domains leads to disease-specific nuances of glutamate-signalling. Curr Top Med Chem. 6: 663–686.

Shepherd GM, Harris KM. 1998. Three-dimensional structure and composition of CA3–>CA1 axons in rat hippocampal slices: implications for presynaptic connectivity and compartmentalization. J Neurosci. 18:8300–8310.

Shepherd GM, Raastad M, Andersen P. 2002. General and variable features of varicosity spacing along unmyelinated axons in the hippocampus and cerebellum. Proc Natl Acad Sci USA. 99:6340–6345.

Small SA, Schobel SA, Buxton RB, Witter MP, Barnes CA. 2011. A pathophysiological framework of hippocampal dysfunction in ageing and disease. Nat Rev Neurosci. 12:585–601.

Spacek J, Harris KM. 1997. Three-dimensional organization of smooth endoplasmic reticulum in hippocampal CA1 dendrites and dendritic spines of the immature and mature rat. J Neurosci. 17:190–203.

Willmann R, Pun S, Stallmach L, Sadasivam G, Santos AF, Caroni P, Fuhrer C. 2006. Cholesterol and lipid microdomains stabilize the postsynapse at the neuromuscular junction. EMBO J. 25:4050–4060.

Zhang J, Petralia RS, Wang YX, Diamond JS. 2016. High-resolution quantitative immunogold analysis of membrane receptors at retinal ribbon synapses. J Vis Exp. (108): 53547. doi: 10.3791/53547.